An oxygen-independent and membrane-less glucose biobattery/supercapacitor hybrid device

Xinxin Xiao, Peter Ó Conghaile, Dónal Leech, Ludwig Roland, EDMOND MAGNER

[Post-print version] To cite this paper: Xinxin Xiao, Peter Ó Conghaile, Dónal Leech, Roland Ludwig, Edmond Magner; An oxygen-independent and membrane-less glucose biobattery/supercapacitor hybrid device, **Biosensors and Bioelectronics 2017**, http://dx.doi.org/10.1016/j.bios.2017.07.023

An oxygen-independent and membrane-less glucose biobattery/supercapacitor hybrid device

Xinxin Xiao[a,*], Peter Ó Conghaile[b, †], Dónal Leech[b], Roland Ludwig[c] and Edmond Magner[a,*]

[a]Department of Chemical Sciences and Bernal Institute, University of Limerick, Limerick, Ireland

[b]School of Chemistry & Ryan Institute, National University of Ireland Galway, Galway, Ireland

[c]Department of Food Science and Technology, BOKU-University of Natural Resources and Life Sciences, Muthgasse 18, 1190 Vienna, Austria

[†]Current address: National Centre for Sensor Research, School of Chemical Sciences, Dublin City University, Dublin 9, Ireland

[*]Corresponding author: Xinxin Xiao (E-mail address: xinxin.xiao@ul.ie); Edmond Magner (E-mail address: edmond.magner@ul.ie; Fax: +353 61 213529; Tel: +353 61 234390)

Abstract

Enzymatic biofuel cells can generate electricity directly from the chemical energy of biofuels in physiological fluids, but their power density is significantly limited by the performance of the cathode which is based on oxygen reduction for *in vivo* applications. An oxygen-independent and membrane-less glucose biobattery was prepared that consists of a dealloyed nanoporous gold (NPG) supported glucose dehydrogenase (GDH) bioanode, immobilised with the assistance of conductive polymer/Os redox polymer composites, and a solid-state NPG/MnO_2 cathode. In a solution containing 10 mM glucose, a maximum power density of 2.3 μW cm^{-2} at 0.21 V and an open circuit voltage

(OCV) of 0.49 V were registered as a biobattery. The potential of the discharged MnO_2 could be recovered, enabling a proof-of-concept biobattery/supercapacitor hybrid device. The resulting device exhibited a stable performance for 50 cycles of self-recovery and galvanostatic discharge as a supercapacitor at 0.1 mA cm^{-2} over a period of 25 h. The device could be discharged at current densities up to 2 mA cm^{-2} supplying a maximum instantaneous power density of 676 μW cm^{-2}, which is 294 times higher than that from the biobattery alone. A mechanism for the recovery of the potential of the cathode, analogous to that of RuO_2 (Electrochim. Acta 42(23), 3541-3552) is described.

Keywords: Biobattery; Enzymatic biofuel cell; Supercapacitor; Hybrid device; Oxygen-independent; Nanoporous gold

1. Introduction

The use of enzymatic biofuel cells (EBFCs) is of promise in generating electricity from fuels (Leech et al. 2012; Rasmussen et al. 2015). EBFCs function at physiological temperature and pH, in comparison to traditional fuel cells utilising abiotic catalysts which generally operate in harsh environments (e.g. strongly acidic or alkaline media). Immobilisation of enzymes at the anode and cathode can eliminate the requirement for membranes that are required in conventional fuel cells to separate the anode and cathode compartments. *In vivo* EBFCs utilising oxygen and glucose are of significant interest due to potential applications as miniaturised power sources for implantable medical devices (Calabrese Barton et al. 2004) such as cardiac pacemakers (MacVittie et al. 2013) and insulin pumps. However, the successful application of autonomous biomedical devices is a significant challenge due to the requirements for high power density, biocompatibility and long lifetime (Shleev 2017). The concentration of oxygen *in vivo* is significantly lower (0.14 mM in arterial blood and 0.08 mM in intestinal tissue (Carreau et al. 2011; Shleev 2017)) than that of glucose (3.3 and 4.8 mM in muscle and plasma, respectively (Maggs et al. 1995)), together with possible mass transport limitation of oxygen, making oxygen reducing biocathode a significant limiting factor in the application of EBFCs. For example, the theoretical power output of an *in vivo* 1 cm long tubular glucose/oxygen EBFC is solely determined by the oxygen reduction reaction (ORR) at the cathode

(Pankratov et al. 2016b). Moreover, the stability of the enzymes used, predominantly multi-copper oxidases such as laccase and bilirubin oxidase (BOx), needs to be considered. Laccase prefers a weakly acidic environment (ca. pH 4-5) and is inhibited by halide ions (Salaj-Kosla et al. 2013; Spira-Solomon et al. 1986; Vaz-Dominguez et al. 2008; Xu 1996). In comparison to laccases, BOx is more stable under physiological conditions (pH 7.4, no inhibition in the presence of Cl^-). However, the operational stability of BOx based electrodes is limited, for example, an osmium polymer "wired" *Trachyderma tsunodae* BOx displayed a current loss of 78% after 2 h rotation at 100 rpm, a loss that was mainly ascribed to the irreversible deactivation of BOx Cu-centers in the oxidised state (Kang et al. 2006).

Air-breathing biocathodes can be employed to circumvent limitations in the supply of oxygen, but can only be used in subcutaneous devices (Miyake et al. 2011). Recently, molecular oxygen-independent hybrid EBFCs or biobatteries relying on a combination of enzymatic anodes and solid-state cathodes have been proposed to address the underlying problems of enzymatic cathode based EBFCs. These abiotic cathodes utilise cheap and abundantly available materials such as Prussian Blue (PB) (Addo et al. 2011), Ag_2O/Ag (Yu et al. 2016b) and MnO_2 (Yu et al. 2016a), which can be reduced/discharged via an external circuit, resulting in rechargeable biobatteries. For example, the oxidation of PB to Berlin Green (BG) occurs at a high potential of 0.87 V vs. SCE (Neff 1985), exceeding the redox potentials of multi-copper oxidases. Minteer et al. developed a rechargeable ethanol biobattery based on an alcohol dehydrogenase (ADH) modified bioanode and a PB paste cathode that registered an open circuit voltage (OCV) of up to 1.2 V (Addo et al. 2011). Dong et al. combined a glucose dehydrogenase (GDH) bioanode with an Ag_2O/Ag (Yu et al. 2016b) or MnO_2 cathode (Yu et al. 2016a) to fabricate oxygen-independent recycled biobatteries with reported OCVs of 0.59 V and 0.43 V, respectively. Microbial biobatteries consisting of anodes colonized by microorganisms and reoxidisable solid-state cathodes such as Ag_2O/Ag (Xie et al. 2013) and PB (Xie et al. 2015) were stable, showing no loss of capacity over 20 cycles of operation (Xie et al. 2015).

Biofuel cell (BFC)/supercapacitor hybrid devices, or self-charging biocapacitors, utilising capacitive bioelectrodes are of great interest due to their ability to generate repeated electric pulses, with an instantaneous power density that is significantly higher than that from the BFC itself (Agnes et al. 2014). Biocapacitors taking advantage of enzymes (Agnes et al. 2014; Kizling et al. 2015; Knoche et al. 2016; Pankratov et al. 2014), microbes (Santoro et al. 2016) and thylakoids (Pankratova et al. 2017) have been presented. Recently, we described a supercapacitive EBFC prepared by the immobilisation of flavin adenine dinucleotide-dependent GDH (FAD-GDH) and BOx with electrodeposited poly(3,4-ethylenedioxythiophene) (PEDOT) and the redox polymer $[Os(2,2'\text{-bipyridine})_2(\text{polyvinylimidazole})_{10}Cl]^{+/2+}$ ($Os(bpy)_2PVI$) on dealloyed nanoporous gold (NPG) (Xiao et al. 2017). The device could operate as a pulse generator to mimic that in a cardiac pacemaker, producing 10 μA pulses for 0.5 ms at a frequency of 0.2 Hz.

In this contribution, we substitute the BOx biocathode with a non-enzymatic MnO_2 cathode to assemble an oxygen-independent glucose biobattery/supercapacitor hybrid device (Scheme 1). At neutral pH MnO_2 only shows catalytic activity towards oxygen at negative potentials (Zhang et al. 2009), outside the potential window needed in this work and is thus used as a consumed cathode. MnO_2 has been selected based on several considerations: (i) a higher pseudo-capacitance in comparison to carbon materials (Simon et al. 2008). MnO_2 is partially charged/discharged via the intercalation/deintercalation of electrolyte cations (e.g. Na^+) and protons according to the reaction:

$$\text{Mn(IV)O}_2 + xNa^+ + yH^+ + (x+y)e^- \leftrightarrow Mn(III)_{(x+y)}Mn(IV)_{1-(x+y)}OONa_xH_y \quad (1)$$

where $0 < (x+y) \leq 1$. In this case, the discharged form is insoluble, avoiding issues with leakage. (ii) a moderate onset potential, resulting in a biobattery with a considerable OCV (Yu et al. 2016a). (iii) operation at neutral pH that is amenable to enzymes. (iv) inert to the oxidation of glucose, as confirmed by Dong et al. (Yu et al. 2016a), resulting in a membrane-less biobattery. A spontaneous recovery of the potential of the discharged NPG/MnO_2 was observed in open-circuit mode, similar to that reported with a pseudo-capacitive RuO_2 electrode (Liu et al. 1997). The assembled NPG/PEDOT/$Os(bpy)_2PVI$/FAD-GDH//NPG/MnO_2 biobattery/supercapacitor hybrid

device delivered intermittent electric signals, with a power density much higher than that of the biobattery itself.

2. Experimental section

2.1. Materials and apparatus

Sodium phosphate (monobasic dehydrate ≥99 % and dibasic ≥99 %), sodium sulfate (≥99.99 %), manganese(II) acetate tetrahydrate (99.99 %), D-(+)-glucose (99.5 %), 3,4-ethylenedioxythiophene (EDOT, 97%) were obtained from Sigma-Aldrich Ireland, Ltd. All solutions were prepared with deionised water (18.2 MΩ cm, Elga Purelab Ultra, UK). $Os(bpy)_2PVI$ was prepared according to an established procedure (Forster et al. 1990; Kober et al. 1988). Oxygen-insensitive, recombinant *Glomerella cingulata* FAD-GDH (EC 1.1.99.10, *D*-glucose: acceptor 1-oxidoreductase) was expressed in *Pichia pastoris* and purified with a specific activity of 572 U mg^{-1} (Sygmund et al. 2011).

Dealloyed NPG leaves were obtained by floating ca. 100 nm thick Au/Ag leaves (12-carat, Eytzinger, Germany) on concentrated HNO_3 (Sigma-Aldrich) for 30 min at 30 °C (Xiao et al. 2015; Xiao et al. 2014). And then placed on well-polished glassy carbon electrodes (GCEs, diameter: 4mm). The NPG electrodes were cleaned by scanning the potential over the range of -0.2 to 1.65 V in 1 M H_2SO_4 at a scan rate of 100 mV s^{-1} for 15 cycles.

Scanning electron microscopy (SEM) images were collected using a Hitachi SU-70 microscope (operating at 15 kV), equipped with an energy dispersive X-ray spectroscopy (EDX). Transmission electron microscopy (TEM, JEOL JEM-2100, operating voltage of 200 kV) images of the electrodes were obtained on samples mounted on 300-mesh copper grids (S147-3, Agar Scientific, UK). The average pore size and layer thickness were measured with ImageJ software (National Institutes of Health, Bethesda, Maryland) (Schneider et al. 2012) using at least 30 measurement points. Raman spectra of MnO_2 deposited on gold foils (thickness: 0.1 mm, purity: 99.9%) were recorded with a LabRAM 300 Raman spectrometer (Horiba Jobin Yvon) using an excitation source at 514 nm (Ar laser).

2.2. Preparation of the enzyme modified anode and NPG/MnO_2 cathode

Electrodeposition was performed in solutions containing phosphate buffer solution (PBS, 0.1 M pH 7.0) containing 2 mM polyethylene glycol 3400 (PEG3400), 20 mM EDOT, 0.5 mg ml^{-1} $Os(bpy)_2PVI$ and 0.5 mg ml^{-1} of FAD-GDH using a pulse sequence of 0.9 V(2 s) and -0.4 V (3 s) for a total time of 300 s (Xiao et al. 2017).

NPG/MnO_2 was fabricated via potentiostatic electrodeposition in 0.1 M Na_2SO_4 and 0.1 M $Mn(CH_3COO)_2$ solution at 0.45 V vs. SCE and 30 °C for certain durations. The as-prepared NPG/MnO_2 electrodes were subsequently immersed in solutions of 1 M H_2SO_4 and deionized water.

2.3. Electrochemical measurements

Electrochemical studies were performed with a CHI802 potentiostat (CH Instruments, Austin, Texas) in a three-electrode electrochemical cell, with the NPG electrode, platinum wire and saturated calomel electrode (SCE) as the working, counter and reference electrodes, respectively. To obtain the power density profile of the assembled biobattery, the bioanode and NPG/MnO_2 cathode were used as the working electrode and combined counter/reference electrode in a two-electrode system. The current was recorded over the potential range open circuit voltage of the BFC to 0 V at a scan rate of 1 mV s^{-1} in N_2-bubbled 0.1 M pH 7.0 PBS containing 10 mM glucose. The power density curve was calculated accordingly. All experiments were carried out at room temperature (20±2 °C) unless stated otherwise.

Testing of the charge/discharge properties of the biobattery was performed in a PBS solution in (0.1 M pH 7.0) containing 10 mM glucose using an Autolab PGSTAT100 potentiostat (Eco Chimie, Netherlands). The NPG/MnO_2 and bioanode were used as working and combined counter/reference electrodes, respectively. The testing sequence comprised (i) stand at open-circuit while recording the open circuit potential (OCP) and (ii) galvanostatic discharge at defined current densities.

3. Results and discussion

3.1. Electrochemical performance of NPG/MnO_2

Anodic deposition is a widely-used method to oxidise Mn(II) dissolved in solution to MnO_2 which is deposited as a film on an electrode (Tench et al. 1983). The specific capacitance of NPG/MnO_2 electrodes increased linearly with deposition time (Fig. S1), in agreement with previous reports (Chen et al. 2013; Kang et al. 2013). The formation of a coating layer was verified by SEM (Fig. S2 and Fig. 1A) and the presence of Mn was confirmed by EDX (Fig. 1B). A Raman band at 657 cm^{-1} was assigned to manganese oxide in the form of Mn(III) and Mn(IV) (Fig. S3) (García et al. 2005). Unmodified NPG had a typical porous structure comprising interconnected pores and ligaments (Xiao et al. 2016), with a uniform diameter of 30.6±5 nm (Fig. S2A). The coating layer obtained after 30 s deposition was not clearly visible in the SEM image (Fig. S2B), but could be clearly identified after deposition for 180 (Fig. 1A) and 300 s (Fig. S2C).

Using TEM, the NPG/MnO_2 composite material could be distinguished by the contrast difference between the modified layer and the gold skeleton (Fig. 1C, Fig. S4). The electrodeposited layer along the pore surfaces showed a relatively uniform thickness of 5.4±1 nm. The previous report, where the same methodology was used but with much thicker coating layers, showed that electrodeposited MnO_2 nanocrystals possess a spinel structure (Kang et al. 2013). Long deposition times, e.g. 300 s, resulted in the formation of thick films that blocked the pores (Fig. S2C), which were likely to be detached from the electrode, leading to significantly degraded operational stability. A deposition period of 180 s was chosen for further electrochemical study. NPG/MnO_2 (180 s) showed an initial specific capacitance of 1.5±0.1 mF cm^{-2}, which was almost four times higher than that of MnO_2 on planar gold obtained using the same procedure and six-fold higher than that of bare NPG (Xiao et al. 2017). NPG/MnO_2 retained 64% of its capacitance, while planar Au/MnO_2 only retained 26% after 50 charge-discharge cycles (Fig. S5) reflecting the role of the substrate NPG in stablising the coating layer due to the confinement effects.

Fig. 1D shows a linear sweep voltammogram (LSV) of NPG/MnO_2 in 0.1 M pH 7.0 PBS, exhibiting a cathodic reduction with an onset potential of ca. +433 mV and a net cathodic current density of 72 μA cm^{-2} at 0.15 V. This reaction was oxygen independent (eq. 1), undergoing insertion of H^+ and Na^+ (Yang et al. 2016). The observed discharge ability enables NPG/MnO_2 to act as a consumed solid-state cathode (Yu et al. 2016a), a potential alternative to ORR active enzymes based biocathodes.

3.2. Electrochemical performance of the bioanode and assembled biobattery

A previously optimised NPG/PEDOT/$Os(bpy)_2$PVI/FAD-GDH bioanode was prepared for the oxidation of glucose (Xiao et al. 2017). Briefly, a pulse sequence consisting of anodic (0.9 V for 2 s) and cathodic -0.4 V (3 s) potentials resulted in the successive deposition of PEDOT and $Os(bpy)_2$PVI with the co-immobilisation of enzyme into the polymer matrix. CVs of the bi-functional electrode displayed a response corresponding to the charge/discharge currents from the capacitive materials and the redox reaction of $Os^{2+/3+}$ (Fig. 2A). The midpoint potential of the osmium redox couple was +210 mV vs. SCE, very close to its reported formal potential of +220 mV vs. Ag/AgCl (Jenkins et al. 2009). On addition of 10 mM glucose, a sigmoidal response (Fig. 2A) arising from the catalytic oxidation of glucose was observed (vide infra, indicative of the immobilisation of FAD-GDH). An onset potential of -18±9 mV vs. SCE was observed.

The NPG/MnO_2 cathode and FAD-GDH based bioanode were assembled and tested without using a membrane. For the first test (blank line, Fig. 2B), the biobattery registered a maximum current density of 14 μA cm^{-2}, a maximum power density of 2.3 μW cm^{-2} at 0.21 V and an OCV of 0.49 V. This performance is an improvement over an equivalent EBFC with a BOx cathode that had a maximum power density of 1.3 μW cm^{-2} and an OCV of 0.46 V (Xiao et al. 2017). A subsequent test (red line, Fig. 2B) showed a decreased power density (max. 1.9 μW cm^{-2}) and OCV (0.39 V) due to partial discharge of MnO_2. To demonstrate the recovery behavior of the cathode, NPG/MnO_2 was then transferred into a three-electrode cell containing PBS and oxidised at 0.5 V vs. SCE for 120 s. The OCV was restored to 0.49 V (blue line, Fig. 2B), the same value of the initial test, with a maximum power density of 2.1 μW cm^{-2}, approaching the initial value. The

recovery of maximum power density and the OCV also implied that the Mn(IV) was reduced to Mn(III) which is insoluble and retained in the film, unlike Mn(II) which is soluble and could diffuse into solution causing unwanted side reactions.

3.3. Electrochemical performance of the hybrid device

The cell was also tested as a hybrid device in N_2-bubbled 10 mM glucose solution. It was reset at the open-circuit mode for 30 min (cut-off at 0.4 V) and subsequently galvanostatic discharged at 0.1 mA cm^{-2} (cut-off at 0 V), a level significantly higher than the discharge current of the biobattery mode (14 μA cm^{-2}). Once the potential of the built-in asymmetric capacitor was discharged to a potential close to zero, interestingly, the potential recovered towards the OCV of the biobattery (Fig. 3A). The mechanism of this is described in the next section. The device could be used for 50 cycles (25 h) of discharge with slight decreases in the onset potential for discharge (in the range of 0.35 and 0.39 V).

The hybrid devices were discharged at various current densities up to 2 mA cm^{-2} (Fig. 3B). Current densities of 1 and 2 mA cm^{-2} led to maximum instantaneous power densities of 378 and 676 μW cm^{-2}, respectively, 164 and 294 times higher than that from a biobattery configuration (2.3 μW cm^{-2}). The significantly improved instantaneous power density was attributed to the intrinsic nature of the supercapacitor. The specific capacitance of the asymmetric supercapacitor was 320 μF cm^{-2} according to the galvanostatic discharge curve. The ohmic resistance during discharge was estimated to be 458 Ω based on the observed voltage drop. The ability to generate high-power-density pules is promising in the development of a hybrid device as a miniaturised power source to generate electric stimuli (e.g. cardiac pacemakers).

Table 1 summarises the performance of representative enzyme based power sources consuming glucose as substrate. In comparison to EBFCs utilising gold nanomaterials including gold nanoparticles (AuNPs) (Wang et al. 2012), highly-ordered macroporous gold (MPG) (Boland et al. 2012) and dealloyed NPG (Siepenkoetter et al. 2017; Xiao et al. 2015) under similar testing conditions, the biobattery displays reasonable output in

terms of maximum power density and OCV. Significantly higher power density was achieved with a carbon nanotube (CNT) based biobattery (Yu et al. 2016a; Yu et al. 2016b), however, this system suffers from the disadvantage that it requires the use of NAD^+ as a cofactor. The performance of the biobattery/supercapacitor hybrid device compares well with that of a biosupercapacitor (Xiao et al. 2017) and with an Os polymer based EBFC/supercapacitor hybrid (Pankratov et al. 2016a) but is lower than that of CNT based hybrid devices in the presence of high glucose concentration (100 and 200 mM) (Agnes et al. 2014; Narvaez Villarrubia et al. 2016).

3.4. Potential recovery of NPG/MnO_2

Conway et al. described the mechanism involved in the recovery of the electrode potential of RuO_2 electrodes that had undergone discharge (Liu et al. 1997). During discharge, the outer region of the metal oxide layer is reduced first, with reduction occurring at a much slower rate in the bulk material due to the limited rate of proton exchange (Ardizzone et al. 1990). The presence of abundant oxidised Ru species in the bulk region enables re-oxidation of the surface region via an electron-hopping/charge transfer mechanism. In an analogous manner, MnO_2 may undergo a similar process. The OCP of the discharged NPG/MnO_2 was examined in a solution that had been saturated with either N_2 or O_2 (Fig. 4A). The potential slowly recovered to ca. 0.37 V in both cases, indicating that the potential recovery was not affected by O_2 over a period of 30 min. Assuming that the electrodeposition of MnO_2 is 100% faradaically efficient (Chen et al. 2013), the amount of deposited MnO_2 can be calculated by integrating the *i*-t curve. Applying a potential of 0.45 V vs. SCE for 180 s resulted in the deposition of 30 nmol MnO_2 onto the NPG. Galvanostatic discharge at 0.1 mA cm^{-2} for a short period of 3 s reduced 0.39 nmol MnO_2 on the surface, assuming that each MnO_2 accepted a single electron (i.e. conversion from Mn(IV) to Mn(III)). This data indicates that each discharge step consumed a very small fraction (1.3%) of the bulk MnO_2. In the open-circuit mode, redistribution of the concentrations of Mn(IV) in the bulk and Mn(III) at the surface leads to the recovery of the potential, in a similar manner as described with RuO_2.

In the discharge step, the OCP of the assembled device decreased rapidly to approach 0 V (Fig. 3A), i.e. a low potential difference between the bioanode and cathode. In the reset step, the charge transfer within the MnO_2 film enabled redistribution of oxidation states that resulted in the return of the potential of the cathode to 0.37 V vs. SCE (Fig. 4A), while the catalytic oxidation of glucose by the bioanode caused the potential to decrease with time to 0.01 V vs. SCE (Fig. 4B) (Pankratov et al. 2016a). Simultaneously, the potential difference allowed the capacitive material on the bioanode to be recharged, whose charge would be released together with the MnO_2 cathode in the next discharge step (Scheme 1).

To emphasise the role of the catalytic active bioanode, we tested a device comprising a NPG/PEDOT anode without FAD-GDH and a NPG/MnO_2 cathode (Fig. S6). The potential recovery was also observed, but with a maximum OCP no higher than 0.1 V, which is lower than that (0.4 V) in the presence of FAD-GDH. Therefore, we confirm that a bioanode is essential to harness the potential difference, making the output potential and power density of the hybrid device acceptable.

4. Conclusions

An oxygen independent and membrane-less glucose biobattery/supercapacitor hybrid device delivering high-power-density pulses was presented. MnO_2 could replace oxygen reducing enzymes as the cathode, due to its features including the capability to be discharged at a reasonable potential, inert to glucose and insoluble reduced state. Most importantly, when only a fraction was discharged in the pulse mode, the spontaneous potential recovery of MnO_2 occurred due to the redistribution of the oxidation states. Coupled with a FAD-GDH based supercapacitive bioanode, the hybrid device function in the similar way of a biosupercapacitor. This biobattery based hybrid device holds promise as an intermittent power source, which can overcome the limited oxygen supply occurring on the conventional biofuel cells, for implanted medical devices.

Acknowledgments

This project has received funding from the European Union's Seventh Framework Programme for research, technological development and demonstration under grant agreement no 607793. X. Xiao acknowledges a Government of Ireland Postgraduate Scholarship (GOIPG/2014/659). P. Ó Conghaile acknowledges a Technology Innovation Development Award through Science Foundation Ireland (15/TIDA/2887).

References

Addo, P.K., Arechederra, R.L., Minteer, S.D., 2011. J. Power Sources 196(7), 3448-3451.
Agnes, C., Holzinger, M., Le Goff, A., Reuillard, B., Elouarzaki, K., Tingry, S., Cosnier, S., 2014. Energy Environ. Sci. 7(6), 1884-1888.
Ardizzone, S., Fregonara, G., Trasatti, S., 1990. Electrochim. Acta 35(1), 263-267.
Boland, S., Leech, D., 2012. Analyst 137(1), 113-117.
Calabrese Barton, S., Gallaway, J., Atanassov, P., 2004. Chem. Rev. 104(10), 4867-4886.
Carreau, A., Hafny-Rahbi, B.E., Matejuk, A., Grillon, C., Kieda, C., 2011. J. Cell. Mol. Med. 15(6), 1239-1253.
Chen, L.Y., Kang, J.L., Hou, Y., Liu, P., Fujita, T., Hirata, A., Chen, M.W., 2013. J. Mater. Chem. A 1(32), 9202-9207.
Forster, R.J., Vos, J.G., 1990. Macromolecules 23(20), 4372-4377.
García, M.A., Ruiz-González, M.L., Quesada, A., Costa-Krämer, J.L., Fernández, J.F., Khatib, S.J., Wennberg, A., Caballero, A.C., Martín-González, M.S., Villegas, M., Briones, F., González-Calbet, J.M., Hernando, A., 2005. Phys. Rev. Lett. 94(21), 217206.
Jenkins, P.A., Boland, S., Kavanagh, P., Leech, D., 2009. Bioelectrochem. 76(1–2), 162-168.
Kang, C., Shin, H., Heller, A., 2006. Bioelectrochem. 68(1), 22-26.
Kang, J., Hirata, A., Kang, L., Zhang, X., Hou, Y., Chen, L., Li, C., Fujita, T., Akagi, K., Chen, M., 2013. Angew. Chem. Int. Ed. 52(6), 1664-1667.
Kizling, M., Draminska, S., Stolarczyk, K., Tammela, P., Wang, Z., Nyholm, L., Bilewicz, R., 2015. Bioelectrochem. 106, Part A, 34-40.
Knoche, K.L., Hickey, D.P., Milton, R.D., Curchoe, C.L., Minteer, S.D., 2016. ACS Energy Lett., 380-385.
Kober, E.M., Caspar, J.V., Sullivan, B.P., Meyer, T.J., 1988. Inorg. Chem. 27(25), 4587-4598.
Leech, D., Kavanagh, P., Schuhmann, W., 2012. Electrochim. Acta 84(0), 223-234.
Liu, T., Pell, W.G., Conway, B.E., 1997. Electrochim. Acta 42(23), 3541-3552.
MacVittie, K., Halamek, J., Halamkova, L., Southcott, M., Jemison, W.D., Lobel, R., Katz, E., 2013. Energy Environ. Sci. 6(1), 81-86.
Maggs, D.G., Jacob, R., Rife, F., Lange, R., Leone, P., During, M.J., Tamborlane, W.V., Sherwin, R.S., 1995. J. Clin. Invest. 96(1), 370-377.
Miyake, T., Haneda, K., Nagai, N., Yatagawa, Y., Onami, H., Yoshino, S., Abe, T., Nishizawa, M., 2011. Energy Environ. Sci. 4(12), 5008-5012.
Narvaez Villarrubia, C.W., Soavi, F., Santoro, C., Arbizzani, C., Serov, A., Rojas-Carbonell, S., Gupta, G., Atanassov, P., 2016. Biosens. Bioelectron. 86, 459-465.
Neff, V.D., 1985. J. Electrochem. Soc. 132(6), 1382-1384.

Pankratov, D., Blum, Z., Suyatin, D.B., Popov, V.O., Shleev, S., 2014. ChemElectroChem 1(2), 343-346.
Pankratov, D., Conzuelo, F., Pinyou, P., Alsaoub, S., Schuhmann, W., Shleev, S., 2016a. Angew. Chem. Int. Ed. 55(49), 15434-15438.
Pankratov, D., Ohlsson, L., Gudmundsson, P., Halak, S., Ljunggren, L., Blum, Z., Shleev, S., 2016b. RSC Adv. 6(74), 70215-70220.
Pankratova, G., Pankratov, D., Hasan, K., Åkerlund, H.-E., Albertsson, P.-Å., Leech, D., Shleev, S., Gorton, L., 2017. Adv. Energy Mater., DOI: 10.1002/aenm.201602285.
Rasmussen, M., Abdellaoui, S., Minteer, S.D., 2015. Biosens. Bioelectron. 76, 91-102.
Salaj-Kosla, U., Pöller, S., Schuhmann, W., Shleev, S., Magner, E., 2013. Bioelectrochem. 91, 15-20.
Santoro, C., Soavi, F., Serov, A., Arbizzani, C., Atanassov, P., 2016. Biosens. Bioelectron. 78, 229-235.
Schneider, C.A., Rasband, W.S., Eliceiri, K.W., Schindelin, J., Arganda-Carreras, I., Frise, E., Kaynig, V., Longair, M., Pietzsch, T., Preibisch, S., 2012. Nat. Methods 9(7), 671.
Shleev, S., 2017. ChemPlusChem, DOI: 10.1002/cplu.201600536.
Siepenkoetter, T., Salaj-Kosla, U., Xiao, X., Conghaile, P.Ó., Pita, M., Ludwig, R., Magner, E., 2017. ChemPlusChem 82(4), 553-560.
Simon, P., Gogotsi, Y., 2008. Nat. Mater. 7(11), 845-854.
Spira-Solomon, D.J., Allendorf, M.D., Solomon, E.I., 1986. J. Am. Chem. Soc. 108(17), 5318-5328.
Sygmund, C., Staudigl, P., Klausberger, M., Pinotsis, N., Djinović-Carugo, K., Gorton, L., Haltrich, D., Ludwig, R., 2011. Microb. Cell Fact. 10(1), 1-9.
Tench, D., Warren, L.F., 1983. J. Electrochem. Soc. 130(4), 869-872.
Vaz-Dominguez, C., Campuzano, S., Rüdiger, O., Pita, M., Gorbacheva, M., Shleev, S., Fernandez, V.M., De Lacey, A.L., 2008. Biosens. Bioelectron. 24(4), 531-537.
Wang, X., Falk, M., Ortiz, R., Matsumura, H., Bobacka, J., Ludwig, R., Bergelin, M., Gorton, L., Shleev, S., 2012. Biosens. Bioelectron. 31(1), 219-225.
Xiao, X., Conghaile, P.Ó., Leech, D., Ludwig, R., Magner, E., 2017. Biosens. Bioelectron. 90, 96-102.
Xiao, X., Magner, E., 2015. Chem. Commun. 51(70), 13478-13480.
Xiao, X., Si, P., Magner, E., 2016. Bioelectrochem. 109, 117-126.
Xiao, X., Ulstrup, J., Li, H., Zhang, J., Si, P., 2014. Electrochim. Acta 130, 559-567.
Xie, X., Ye, M., Hsu, P.-C., Liu, N., Criddle, C.S., Cui, Y., 2013. Proc. Natl. Acad. Sci. 110(40), 15925-15930.
Xie, X., Ye, M., Liu, C., Hsu, P.-C., Criddle, C.S., Cui, Y., 2015. Energy Environ. Sci. 8(2), 546-551.
Xu, F., 1996. Biochemistry 35(23), 7608-7614.
Yang, L., Cheng, S., Wang, J., Ji, X., Jiang, Y., Yao, M., Wu, P., Wang, M., Zhou, J., Liu, M., 2016. Nano Energy 30, 293-302.
Yu, Y., Han, Y., Lou, B., Zhang, L., Han, L., Dong, S., 2016a. Chem. Commun. 52(92), 13499-13502.
Yu, Y., Xu, M., Bai, L., Han, L., Dong, S., 2016b. Biosens. Bioelectron. 75, 23-27.
Zhang, L., Liu, C., Zhuang, L., Li, W., Zhou, S., Zhang, J., 2009. Biosens. Bioelectron. 24(9), 2825-2829.

Figures and captions

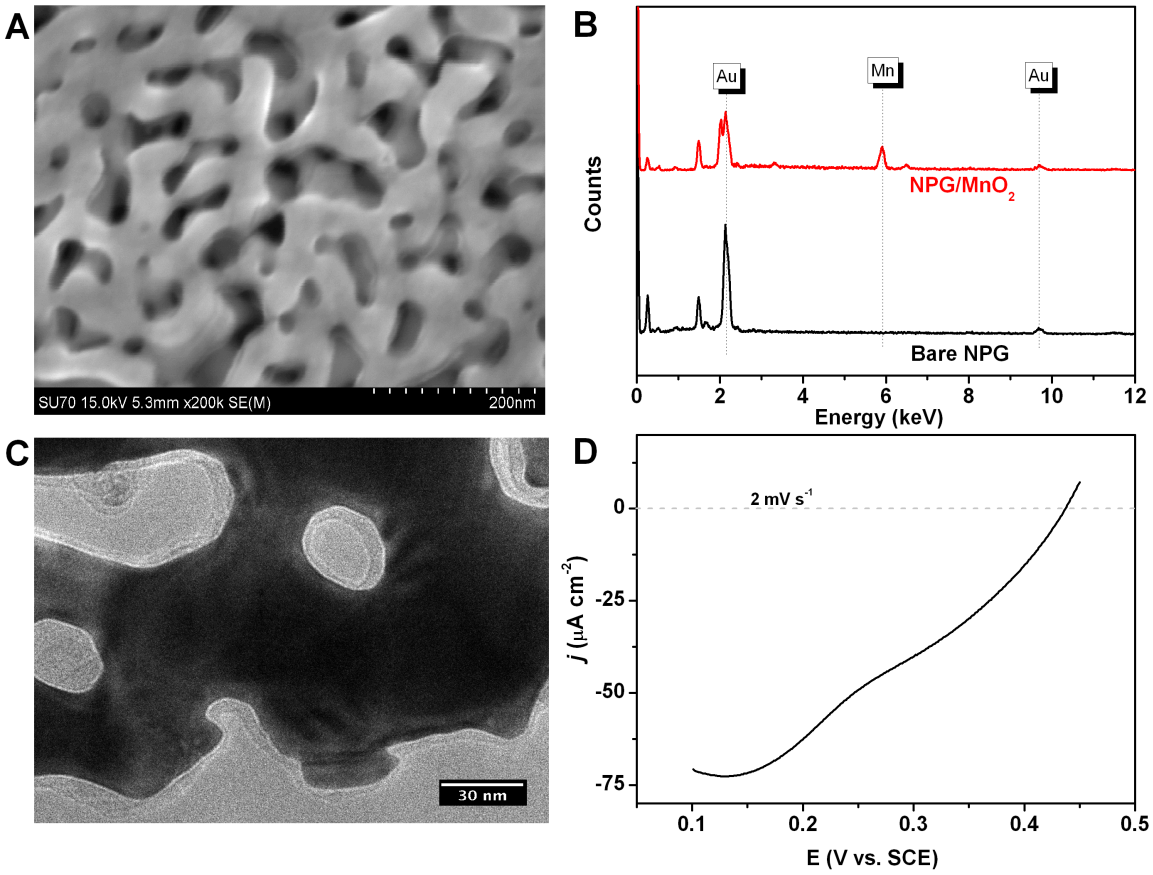

Fig. 1. SEM (A) and TEM (C) image of NPG/MnO_2 (deposition time: 180 s). (B) EDX spectra of bare NPG and NPG/MnO_2 (deposition time: 180 s). (D) LSV of NPG/MnO_2 (deposition time: 180 s) in 0.1 M pH 7.0 PBS at a scan rate of 2 mV s^{-1}.

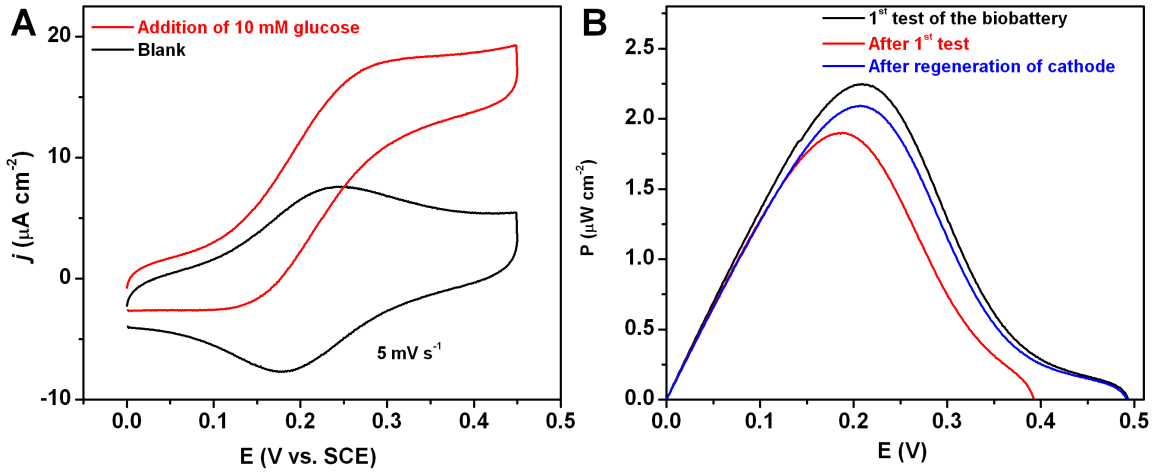

Fig. 2. (A) CVs of the NPG/PEDOT/Os(bpy)$_2$PVI/FAD-GDH bioanode. (B) The performance of the biobattery in the presence of 10 mM glucose.

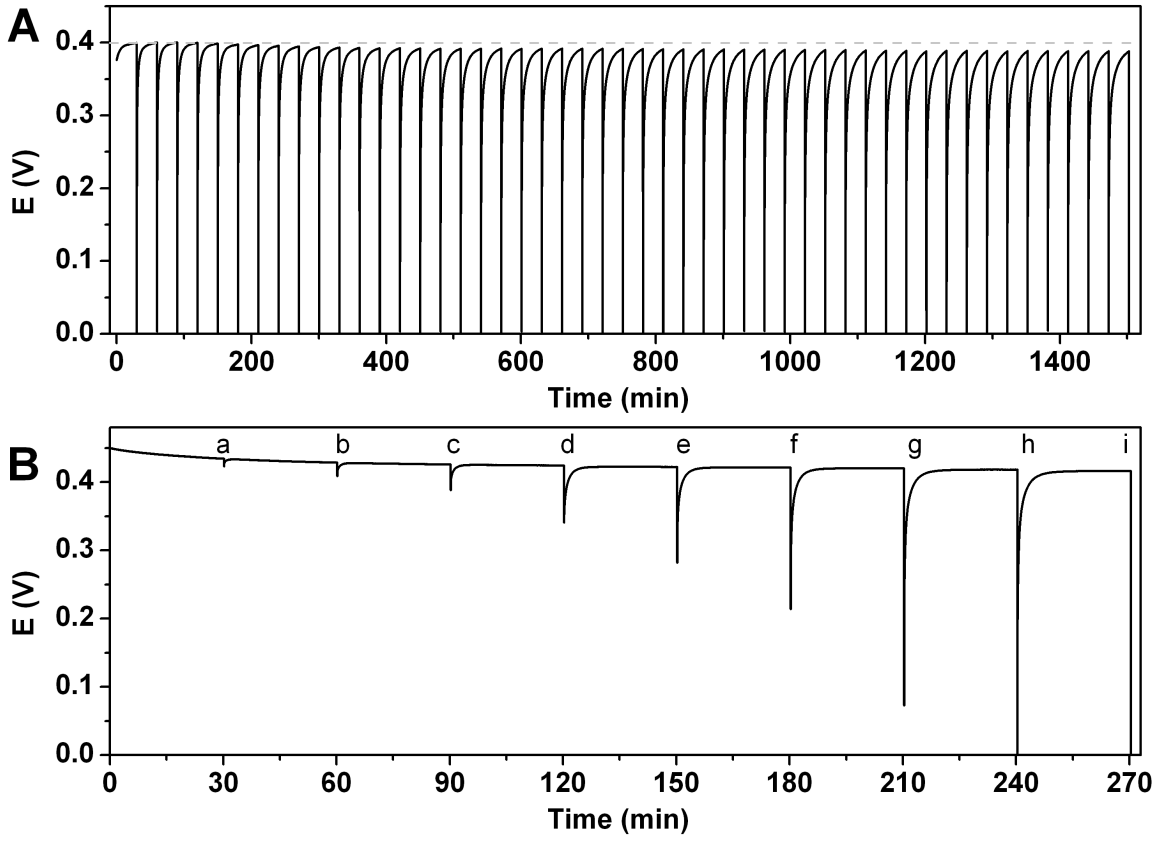

Fig. 3. (A) Potential profile of the device for 50 cycles. Solution: 0.1 M 7.0 PBS and 10 mM glucose. Experimental protocol: reset at open-circuit for 30 min and cutoff at 0.4 V, followed by discharging at 0.1 mA cm^{-2} and cutoff at 0 V. (B) Charge/discharge curves of the biocapacitor upon various discharging current densities; Experimental setup: reset at open-circuit for 30 min, followed by discharging at 0.005 (a), 0.01 (b), 0.02 (c), 0.05 (d), 0.1 (e), 0.2 (f), 0.5 (g), 1 (h), 2 (i) mA cm^{-2} for 0.2 s and cutoff at 0 V.

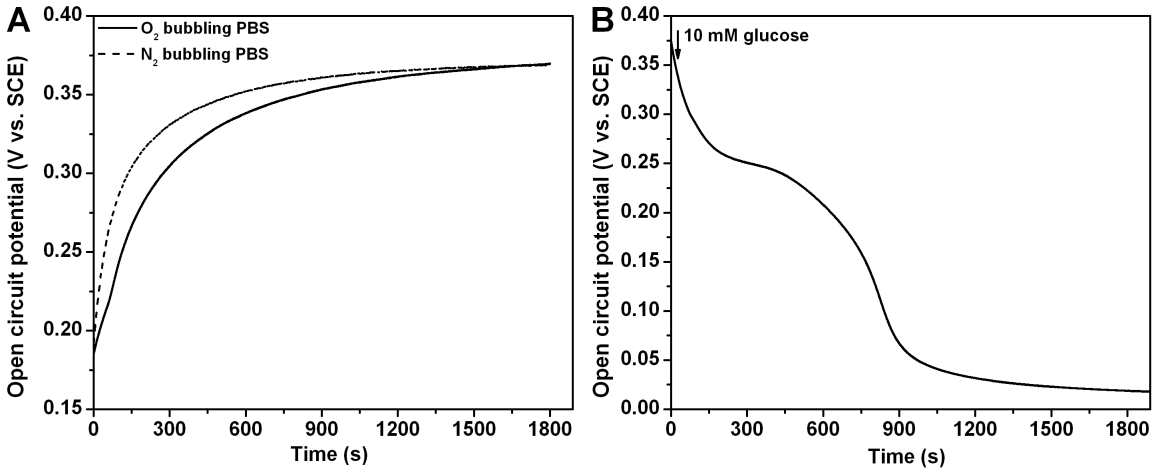

Fig. 4. (A) OCP of NPG/MnO_2 in the presence of N_2 or O_2. The electrode was discharged by scanning potential from 0.5 to 0 V vs. SCE at a scan rate of 1 mV s^{-1}. (B) OCP of the bioanode upon the addition of 10 mM glucose.

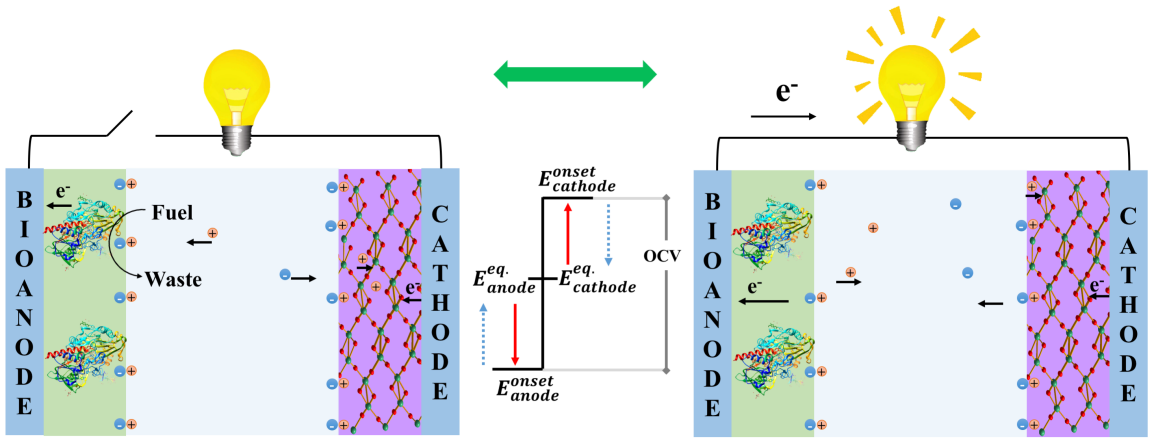

Scheme 1. Schematic diagrams of the hybrid device working at the reset (left) and galvanostatic discharging mode (right). The scheme in the middle depicts the relevant potential differences, with potential shifts caused by galvanostatic discharging (blue arrows) and on the recovery of the potential during the quiescent step (red arrows).

Table 1. List of properties of enzymatic power sources utilising glucose as substrate.

Power source	Anode	Cathode	[Glucose] (mM)	OCV (V)	P_{Max} (μWcm^{-2})	Stability	Ref.
Au electrode based EBFC	Au/AuNPs/*Ct*CDH	Au/AuNPs/*Mv*BOx	5	0.68	3.3	~20% drop in 12 h of continuous operation	(Wang et al. 20
	MPG/ $Os(dmbpy)_2PVI$/*An*GOx	MPG/ $Os(bpy)_2PVI$/ *Ma*Lc	10	~0.52	38	N/A	(Boland et a 2012)
	NPG/ $Os(dmbpy)_2PVI$/*An*G Ox	NPG/ $Os(bpy)_2PVI$/ *Mv*BOx	5	0.56	3.65	25% drop in 12 h of storage	(Xiao et al. 20
	NPG/ $Os(bpy)_2PVI$/FAD-GDH	NPG-*Mv*BOx	5	0.45	17.5	~40% drop in 8 h of continuous operation	(Siepenkoette al. 2017)
Biobattery	CFP/ NAD^+-IL-SWCNTs/GDH/CS	GF/ MnO_2	30	0.43	40.5	N/A	(Yu et al. 201
	GCE/MWCNTs/MDB/GD H	Ag_2O/Ag	30	0.59	275	Less than 50% drop in 6 h of continuous operation	(Yu et al. 201
EBFC/SC hybrid	MWCNTs/*An*GOx/catalase	MWCNTs/Lc	200	1±0.1	EBFC: 16 mW Hybrid: N/A	Charge/discharge for 5 days at 3 mA	(Agnes et al. 2(
	NPG/PEDOT/ $Os(bpy)_2PVI$/ FAD-GDH	NPG/PEDOT/ $Os(bpy)_2PVI$/*Mv*BOx	10	0.46	EBFC: 1.3 Hybrid: 608.8	50 cycles charge/discharge for ~7 h at 0.2 mA cm^{-2}	(Xiao et al. 20
	Graphite/Os polymer/PQQ-GDH	Graphite/Os polymer/*Mv*BOx	20	0.45	EBFC: ~3 Hybrid: N/A	Charge/discharge for ~50 h	(Pankratov et 2016a)

	BP/MWCNTs/pMG/GDH Diffusing NAD^+	BP/MWCNTs/BOx	100	~0.56	EBFC: N/A Hybrid: 1070	Charge/discharge for 3 days at 0.4 mA cm^{-2}	(Narvaez Villarrubia et 2016)
Biobattery/SC hybrid	NPG/PEDOT/$Os(bpy)_2PVI$/ FAD-GDH	NPG/MnO_2	10	0.49	Biobattery: 2.3 Hybrid: 676	50 cycles charge/discharge for ~25 h at 0.1 mA cm^{-2}	This work

CDH: cellobiose dehydrogenase; $Os(dmbpy)_2PVI$: $[Os(4,4'\text{-dimethyl-}2,2'\text{-bipyridine})_2(\text{polyvinylimidazole})_{10}Cl]^{+/2+}$; GOx: glucose oxidase; Lc: laccase; N/A: not available; SC: supercapacitor; MWCNTs: multi-walled carbon nanotubes; BP: buckypaper; pMG: polymerized methylene green; MDB: Meldola's blue; CFP: carbonfiber paper; SWCNTs: single-walled carbon nanotubes; IL: ionic liquid; CS: chitosan; GF: graphite flake.